

# Articulated Multi-person Tracking in the Wild

Eldar Insafutdinov, Mykhaylo Andriluka, Leonid Pishchulin, Siyu Tang,  
Evgeny Levinkov, Bjoern Andres, Bernt Schiele

Max Planck Institute for Informatics  
Saarland Informatics Campus  
Saarbrücken, Germany

## Abstract

*In this paper we propose an approach for articulated tracking of multiple people in unconstrained videos. Our starting point is a model that resembles existing architectures for single-frame pose estimation but is several orders of magnitude faster. We achieve this in two ways: (1) by simplifying and sparsifying the body-part relationship graph and leveraging recent methods for faster inference, and (2) by offloading a substantial share of computation onto a feed-forward convolutional architecture that is able to detect and associate body joints of the same person even in clutter. We use this model to generate proposals for body joint locations and formulate articulated tracking as spatio-temporal grouping of such proposals. This allows to jointly solve the association problem for all people in the scene by propagating evidence from strong detections through time and enforcing constraints that each proposal can be assigned to one person only. We report results on a public MPII Human Pose benchmark and on a new dataset of videos with multiple people. We demonstrate that our model achieves state-of-the-art results while using only a fraction of time and is able to leverage temporal information to improve state-of-the-art for crowded scenes<sup>1</sup>.*

## 1. Introduction

This paper addresses the task of articulated human pose tracking in monocular video. We focus on scenes of realistic complexity that often include fast motions, large variability in person appearance and clothing styles, and person-person occlusions. A successful approach should thus be able to identify the number of people present in each video frame, determine locations of the joints of each person and cor-



Figure 1. Example articulated tracking results of our approach.

rectly associate the body joints over time.

One of the key challenges in such scenes is that people might overlap and only a subset of joints of the person might be visible in each frame either due to person-person occlusion or truncation by image boundaries (*c.f.* Fig. 1). Arguably, resolving such cases correctly requires reasoning beyond purely geometric information on the arrangement of body joints in the image, and requires incorporation of a variety of image cues and joint modeling of several human subjects.

The design of our model is motivated by two factors. We would like to leverage bottom-up end-to-end learning to directly capture image information. At the same time we aim to address a complex prediction problem of multi-person articulated tracking that does not naturally lend itself to an end-to-end prediction task and for which training data is not available in the amounts usually required for end-to-end learning.

To leverage the available image information we learn a model for associating a body joint to a specific person in an end-to-end fashion relying on a convolutional network. We then incorporate these part-to-person association responses into a framework for jointly reasoning about assignment of body joints within the image and over time. To that end we use the graph partitioning formulation that has been used for people tracking and pose estimation in the past [21, 19], but has not been shown to enable articulated people tracking.

<sup>1</sup>Models and the dataset will be made publicly available.

To facilitate efficient inference in video we resort to fast inference methods based on local combinatorial optimization [16] and aim for a sparse model that keeps the number of connections between variables to a minimum. As we demonstrate, in combination with feed-forward reasoning for joint-to-person association this allows us to achieve speed-ups of several orders of magnitude compared to state-of-the-art [12] while maintaining the same level of accuracy.

The key contribution of this work is a new model for articulated tracking that operates by bottom-up assembly of part detections within each frame and over time. Contrary to existing work such as [10, 18] this model is suitable for scenes with an unknown number of subjects and performs reasoning jointly across multiple people incorporating inter-person exclusion constraints and propagating strong observations to neighboring frames.

Our second contribution is a formulation for single-frame pose estimation that relies on a sparse graph between body parts and a mechanism for generating body-part proposals conditioned on a person’s location. This is in contrast to state-of-the-art approaches [19, 12] that perform expensive inference in a full graph and rely on generic bottom-up proposals. We demonstrate that a sparse model with a few spatial edges performs competitively with a fully-connected model while being much more efficient. Notably, a simple model that operates in top-down/bottom-up fashion exceeds the performance of a fully-connected model while being 24x faster at inference time (cf. Tab. 3). This is due to offloading of a large share of the reasoning about body-part association onto a feed-forward convolutional architecture.

Finally, we contribute a new challenging dataset for evaluation of articulated body joint tracking in crowded realistic environments with multiple overlapping people. Our models and a new dataset will be made publicly available.

**Related work.** Convolutional networks have emerged as an effective approach to localizing body joints of people in images [24, 25, 17, 12] and have also been extended for joint estimation of body configurations over time [10].

Current approaches are increasingly effective on the task of estimating body configurations of single people [24, 25, 17, 4, 10] achieving high accuracies on this task, but are still failing on fast moving and articulated limbs. More complex recent models are able to jointly work with entire scenes [19, 12], but are too complex and inefficient to be directly generalizable to perform reasoning across the entire video. [14] propose an efficient approach to multi-person pose estimation that relies on greedy inference prone to local optima. Recent feed-forward models are able to jointly infer body joints of the same person and even operate over time [10] but consider isolated persons only and do not generalize to the case of multiple overlapping people. Similarly, [5, 18] consider a simplified task of tracking upper body poses of isolated upright individuals.

Recently, [8, 9] proposed an approach that aims at generalizing from a studio-based motion capture setting to the outdoor environments. However, they require multiple views of the same scene and are only able to simultaneously track poses of a low number of persons (1-2 typically). In contrast, we focus on monocular video sequences and propose an approach to tracking arbitrary number of highly articulated people.

We build on recent convnet detectors [12] that have been shown to be effective in localizing body joints even in the presence of clutter and explore different mechanisms for assembling the joints into multiple person configurations. To that end we rely on a graph partitioning approach closely related to [21, 19, 12]. However, in contrast to [21] who focus on pedestrian tracking, and [19, 12] who perform single frame based multi-person pose estimation, we go beyond and solve much more complex problem of articulated multi-person pose tracking. In contrast to [19, 12] that perform expensive inference in the full graph we employ much more efficient approaches based on sparse graph representations and novel person conditioned top-down bottom-up reasoning.

Earlier approaches to articulated pose tracking in monocular videos rely on hand-crafted image representations and focus on either of simplified tasks, such as tracking upper body poses of frontal isolated people [20, 27, 23, 7], or tracking walking pedestrians with little degree of articulation [2, 3]. In contrast, we address much harder problem of multi-person highly-articulated pose tracking and heavily rely on learning representations from image pixels by offloading the larger share of the reasoning about body-part association onto feed-forward convolutional architecture.

**Overview.** Our model consists of the two components: (1) a convolutional network for generating body part proposals and (2) an approach to group the proposals into spatio-temporal clusters. In Sec. 2 we proceed by introducing a general formulation for multi-target tracking that follows [21] and allows us to define pose estimation and articulated tracking in a unified framework. We then describe the details of our articulated tracking approach in Sec. 3, and introduce two variants of our formulation: bottom-up (*BU*) and top-down/bottom-up (*TD/BU*). We present experimental results in Sec. 4.

## 2. Tracking by Spatio-temporal Grouping

Our body part detector generates a set of proposals  $D = \{\mathbf{d}_i\}$  for each frame of the video. Each proposal is given by  $\mathbf{d}_i = (t_i, d_i^{pos}, \pi_i, \tau_i)$ , where  $t_i$  denotes the index of the video frame,  $d_i^{pos}$  is the spatial location of the proposal in image coordinates,  $\pi_i$  is the probability of correct detection, and  $\tau_i$  is the type of the body joint (*e.g.* ankle or shoulder).

Let  $G = (D, E)$  be a graph whose nodes  $D$  are the body-part proposals of an entire video and whose edges  $E$  con-

nect pairs of detections that hypothetically correspond to the same target.

The output of the tracking algorithm is a subgraph  $G' = (D', E')$  of  $G$ , where  $D'$  is a subset of nodes after filtering redundant and erroneous detection hypotheses and  $E'$  are edges linking nodes corresponding to the same target. We specify  $G'$  via binary indicator variables  $x \in \{0, 1\}^D$  and  $y \in \{0, 1\}^E$  that define subsets of edges and nodes included in  $G'$ . In particular each track will correspond to a connected component in  $G'$ .

As a general way to introduce constraints on edge configurations that correspond to a valid tracking solution we introduce a set  $Z \subseteq \{0, 1\}^{D \cup E}$  and define a combination of edge and node indicator variables to be feasible if and only if  $(x, y) \in Z$ . An example of a constraint encoded through  $Z$  is that endpoint nodes of an edge included by  $y$  must also be included by  $x$ . Note that the variables  $x$  and  $y$  are coupled though  $Z$ . Moreover, assuming that  $(x, y) \in Z$  we are free to set components of  $x$  and  $y$  independently to maximize the tracking objective.

Given image observations we compute a set of features for each node and edge in the graph. We denote such node and edge features as  $f$  and  $g$  respectively. Assuming independence of the feature vectors the conditional probability of indicator functions  $x$  of nodes and  $y$  of edges given features  $f$  and  $g$  and given a feasible set  $Z$  is given by

$$p(x, y | f, g, Z) \propto p(Z | x, y) \prod_{d \in D} p(x_d | f^d) \prod_{e \in E} p(y_e | g^e), \quad (1)$$

where  $p(Z | x, y)$  assigns a constant non-zero probability to every feasible solution and is equal to zero otherwise. Minimizing the negative log-likelihood of Eq. 1 is equivalent to solving the following integer-linear program:

$$\min_{(x, y) \in Z} \sum_{d \in D} c_d x_d + \sum_{e \in E} d_e y_e, \quad (2)$$

where  $c_d = \log \frac{p(x_d=1 | f^d)}{p(x_d=0 | f^d)}$  is the cost of retaining  $d$  as part of the solution, and  $d_e = \log \frac{p(y_e=1 | g^e)}{p(y_e=0 | g^e)}$  is the cost of assigning the detections connected by an edge  $e$  to the same person track.

We define the set of constraints  $Z$  as in [21]:

$$\forall e = vw \in E : y_{vw} \leq x_v \quad (3)$$

$$\forall e = vw \in E : y_{vw} \leq x_w \quad (4)$$

$$\forall C \in \text{cycles}(G) \forall e \in C : (1 - y_e) \leq \sum_{e' \in C \setminus \{e\}} (1 - y_{e'}) \quad (5)$$

Jointly with the objective in Eq. 2 the constraints (3)-(5) define an instance of the minimum cost subgraph multicut

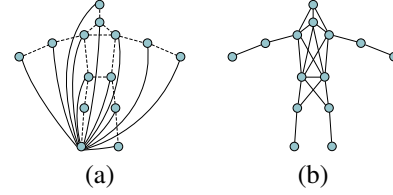


Figure 2. Different connectivity types. (a): fully connected graph as in [19, 12]; (b): sparse graph. For fully connected graph only a subset of edges is shown.

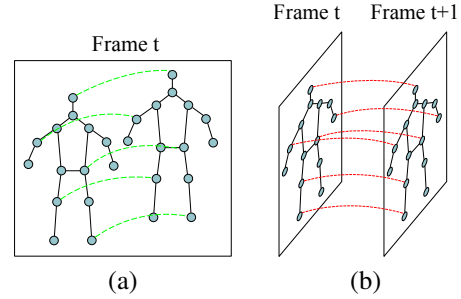


Figure 3. Visualization of attractive-repulsive and temporal edges in our model. We show only a subset of attractive/repulsive and temporal edges for clarity.

problem [21]. The constraints (3) and (4) ensure that assignment of node and edge variables is consistent. The constraint (5) ensures that for every two nodes either all or none of the paths between these nodes in graph  $G$  are contained in one of the connected components of subgraph  $G'$ . This constraint is necessary to unambiguously assign person identity to a body part proposal based on its membership in a specific connected component of  $G'$ .

### 3. Articulated Multi-person Tracking

In Sec. 2 we introduced a general framework for multi-object tracking by solving an instance of the subgraph multicut problem. The subgraph multicut problem is NP-hard, but recent work [21, 16] has shown that efficient approximate inference is possible with local search methods. The framework allows for a variety of graphs and connectivity patterns. Simpler graph connectivity will usually allow for faster and more efficient processing at the cost of ignoring some of the potentially informative dependencies between model variables. Our goal is to design a model that is efficient, with as few edges as possible, yet effective in crowded scenes with many people and allowing us to model temporal continuity and inter-person exclusion. Our articulated tracking approach proceeds by constructing a graph  $G$  that couples body part proposals within the same frame and across neighboring frames. In general the graph  $G$  is going to have three types of edges:

- *cross-type* pairwise terms shown in Fig. 2 and 5 (b) that connect two parts of different types

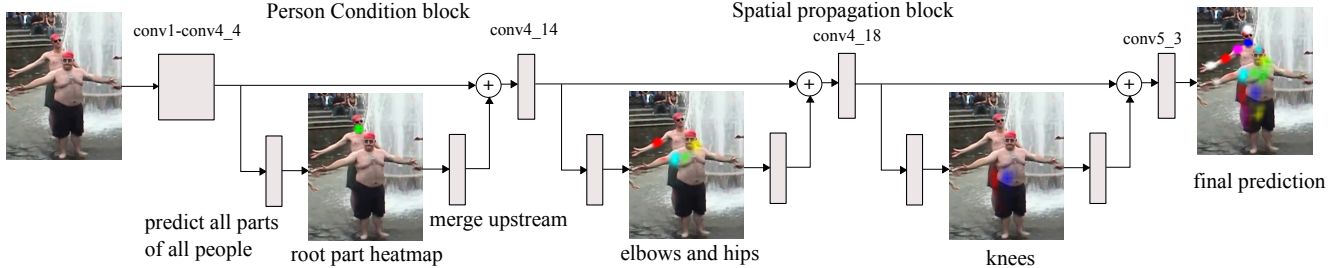


Figure 4. CNN architecture for computing person conditioned proposals and pairwise terms. *SP* block for shoulders at *conv4\_8* is omitted for clarity.

- *same-type* pairwise terms shown in Fig. 3 (a) connect two nodes of the same type in the same image
- *temporal* pairwise terms shown in Fig. 3 (b) that connect nodes in the neighboring frames.

We now define two variants of our model which we denote as *Bottom-Up (BU)* and *Top-Down/Bottom-Up (TD/BU)*. These models rely on the identical *same-type* and *temporal* pairwise terms, but differ with respect to mechanism for proposal generation, the form of *cross-type* pairwise terms, and connectivity of nodes in  $G$ . For both models we will rely on the solver from [16] for inference.

### 3.1. Bottom-Up Model (BU).

In the *Bottom-Up* model the detection proposals are generated by a convolutional part detector. We use off-the-shelf code made publicly available by the authors of [12]<sup>2</sup>. For each body part proposal  $\mathbf{d}_i$  the detector outputs image location, probability of detection  $\pi_i$ , and a label  $\tau_i$  that indicates the type of the detected body part (*e.g.* shoulder or ankle). We directly use the probability of detection to derive the unary costs in Eq. 2 as  $c_{d_i} = \log(\pi_i / (1 - \pi_i))$ . Image features  $f^d$  in this case correspond to the image representation generated by the convolutional network.

We consider two connectivity patterns for nodes in the graph  $G$ . We either define edges for every pair of proposals which results in a fully connected graph between proposals in each image as is shown in Fig. 2 (a). Alternatively we obtain a sparse version of the model by defining edges for a subset of part types only as is shown in Fig. 2 (b). The rationale behind the sparse version is to obtain a cleaner and faster version of the model by omitting edges between parts that carry little information about each other’s image location (*e.g.* left ankle and right arm).

**Edge costs.** In our *Bottom-Up* model the cost of the edges  $d_e$  connecting two body part detections  $\mathbf{d}_i$  and  $\mathbf{d}_j$  is defined as a function of the detection types  $\tau_i$  and  $\tau_j$ . Following [12] we thus train for each pair of part types a regression function that predicts relative image location of the parts in the pair. The cost  $d_e$  is given by the output of the logistic regression

given the features computed from offset and angle of the predicted and actual location of the other joint in the pair. We refer to [12] for more details on these pairwise terms.

Note that our model generalizes [21] in that the edge cost depends on the type of nodes being connected by the edge. It also generalizes [19, 12] by allowing  $G$  to be sparse. This is achieved by reformulating the model with a more general type of cycle constraint (5), in contrast to simple triangle inequalities used in [19, 12]<sup>3</sup>.

### 3.2. Top-Down/Bottom-up Model (TD/BU)

We now introduce a version of our model that operates by first generating body part proposals conditioned on the locations of people in the image and then performing joint reasoning to group these proposals into spatio-temporal clusters corresponding to different people. Here we follow the intuition that it is considerably easier to identify and detect individual people (*e.g.* by detecting their heads) compared to correctly associating body parts such as ankles and wrists to each person. We select person’s head as the root part that is responsible for representing the person location, and delegate the task of identifying body parts of the person corresponding to a head location to a convolutional network.

For head detection, we use a simplified version of our model that contains the two head parts (chin and “head top”). This makes our *TD/BU* model related to the hierarchical model defined in [12] that also uses easier-to-detect parts to condition the rest of the inference process. However here we replace all the stages in the hierarchical inference except the first stage with the feed-forward convolutional network.

The structure of our *TD/BU* model is illustrated in Fig. 5 (b) for the simplified case of two distinct head detections. Let us denote the set of all root part detections as  $D^{root} = \{d_i^{root}\}$ . For each pair of the root nodes we explicitly set the corresponding edge indicator variables  $y_{d_j^{root}, d_k^{root}} = 0$ . This implements a “must-not-link” constraint between these nodes, and in combination with the cycle inequality (5) implies that each proposal can be connected to one of the “per-

<sup>2</sup><http://pose.mpi-inf.mpg.de/>

<sup>3</sup>See Sec. 2.1 in [19]

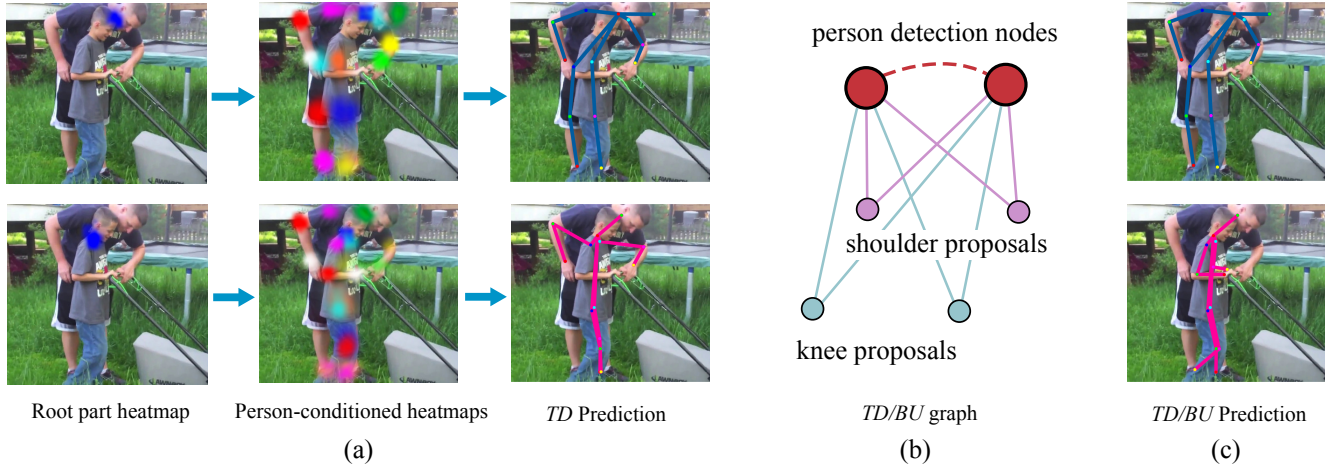


Figure 5. (a) Processing stages of the *Top-Down* model shown for an example with significantly overlapping people. Left: Heatmaps for the chin (=root part) used to condition the CNN on the location of the person in the back (top) and in the front (bottom). Middle: Output heatmaps for all body parts, notice the ambiguity in estimates of the arms of the front person. Right: *TD* predictions for each person. (b) Example of the *Top-Down/Bottom-Up* graph. Red dotted line represents the must-cut constraint. Note that body part proposals of different type are connected to person nodes but not between each other. (c) *Top-Down/Bottom-Up* predictions. Notice that the *TD/BU* inference correctly assigns the forearm joints of the frontal person.

son nodes” only. We define the cost for an edge connecting detection proposal  $\mathbf{d}_k$  and a “person node”  $d_i^{root}$  based on the conditional distribution  $p_{d_k^c}(d_k^{pos} | d_i^{root})$  generated by the convolutional network. The output of such network is a set of conditional distributions, one for each node type. We augment the graph  $G$  with attractive/repulsive and temporal terms as described in Sec. 3.3 and Sec. 3.4 and set the unary costs for all indicator variables  $x_d$  to a constant. We consider a proposal to be excluded from the final solution if it is not connected to any of the root nodes. We use the solver from [16] for consistency, but a simpler KL-based solver as in [21] could be used as well since the *TD/BU* model effectively ignores the unary variables  $x_d$ . We illustrate the processing stages of the *TD/BU* model in Fig. 5. Note that the body-part heatmaps change substantially depending on the person-identity signal provided by the person’s chin, and that the bottom-up step was able to correct the predictions on the forearms of the front person.

**Model details.** In the following we provide the details of training the convolutional network that generates the conditional distributions. The structure of the convolutional network is shown on Fig. 4. The network resembles the ResNet-101 architecture from [11], which we modify as in [12] to bring the stride of the full network down to 8px. This is achieved by using dilated convolutions [6] in conv5 bank and up-convolutional layers with stride 2 in the final layer.

We place a cross-entropy classification loss layer ( $N$  binary classifications) that indiscriminately predicts all parts of all people in the image at the *conv4.4* block of the network. At each training iteration we forward pass an image with multiple people potentially in close proximity to each other. We select a single person from the image and condi-

tion the network on the head location of that person. This is achieved by masking out the prediction heat-map of the root joint around its ground truth location on the given person. We then map the prediction maps to match the dimensionality of the feature channels and add them to the main stream of the ResNet. We finally add a part prediction layer at the top of the network with a loss that considers predictions to be correct only if they correspond to body parts of the selected person.

**Spatial propagation (SP).** In our network the person identity signal is provided by the location of the head. In principle the receptive field size of the network is large enough to propagate this signal to all body parts<sup>4</sup>. However we found that it is useful to introduce an additional mechanism to propagate the person identity signal. To that end we inject intermediate supervision layers for individual body parts arranged in the order of kinematic proximity to the root joint (Figure 4). We place prediction layers for shoulders at *conv4\_8*, for elbows and hips at *conv4\_14* and for knees at *conv4\_18*. We empirically found that such an explicit form of spatial propagation significantly improves performance on joints such as ankles, that are typically far from the head in the image space (see Tab. 2 for details).

<sup>4</sup>In our network the root part location is specified at the layer *conv4.4*. Between this layer and the top of the network there are  $N_1 = 18$  layers in the *conv4* bank and  $N_2 = 3$  layers of *conv5* bank that run at stride *stride* = 16px. The receptive field at the top prediction layer with respect to injection of the person condition signal is given by  $stride \times (k_1 - 1) \times N_1 + stride \times (k_2 - 1) \times N_2$  where  $k_1 = 3$  is the size of kernels in each residual block in *conv4* and  $k_2 = 5$  is the effective size of the kernel in *conv5* taking into account the dilated convolution. Therefore the total receptive field is 768px. We scale our train and test images such that average height of a person is 340px so the receptive field is large enough to allow for the information from the head to propagate to lower body.

**Training.** We use Caffe’s [15] ResNet implementation and initialize from the ImageNet-pre-trained models. Networks are trained on the MPII Human Pose dataset [1] with SGD for 1M iterations with stepwise learning rate (lr=0.002 for 400k, lr=0.0002 for 300k and lr=0.0001 for 300k).

### 3.3. Attractive/Repulsive Edges

Attractive/repulsive edges are defined between two proposals of the same type within the same image. The costs of these edges are given by a logistic classifier that takes distance between proposals as a feature and assigns an increasingly low probability to edges between proposals that are far from each other [12]. This achieves an effect similar to non-maximum suppression but the decision to group two nodes is made based on evidence from the entire image and not just the state of two detection proposals. Inversely, these terms prevent grouping of multiple distant hypothesis of the same type, e.g. preventing two proposals for the person’s head to be assigned to the same person.

### 3.4. Temporal Model

Regardless of the type of within frame model (*BU* or *TD/BU*) we rely on the same type of temporal edges that connect nodes of the same type in adjacent frames. We derive the costs for such temporal edges via logistic regression. Given the feature vector  $g_{ij}$  the probability that the two proposals  $\mathbf{d}_i$  and  $\mathbf{d}_j$  in adjacent frames correspond to the same body part is given by:

$$p(y_{ij} = 1 | g_{ij}) = \frac{1}{1 + \exp(-\langle \omega_t, g_{ij} \rangle)}, \quad (6)$$

where  $g_{ij} = (\Delta_{ij}^{L2}, \Delta_{ij}^{Sift}, \Delta_{ij}^{DM}, \tilde{\Delta}_{ij}^{DM})$ , and  $\Delta_{ij}^{L2} = \|d_i^{pos} - d_j^{pos}\|_2$ ,  $\Delta_{ij}^{Sift}$  is Euclidean distance between the SIFT descriptors computed at  $d_i^{pos}$  and  $d_j^{pos}$ , and  $\Delta_{ij}^{DM}$  and  $\tilde{\Delta}_{ij}^{DM}$  measure the agreement with the dense motion field computed with the DeepMatching approach of [26]. In the evaluation in Tab. 5 we refer to these features as *det-distance*, *sift-distance* and *deepmatch* respectively.

For SIFT features we specify the location of the detection proposal, but rely on SIFT to identify the local orientation. In cases with multiple local maxima in orientation estimation we compute SIFT descriptor for each orientation and set  $\Delta_{ij}^{Sift}$  to the minimal distance among all pairs of descriptors. We found that this makes the SIFT distance more robust in the presence of rotations of the body limbs.

We define the features  $\Delta_{ij}^{DM}$  and  $\tilde{\Delta}_{ij}^{DM}$  inspired by [22]. For each part proposal  $\mathbf{d}_i$  we define a corresponding image region  $R_i = R(\mathbf{d}_i)$  that covers the image area between the proposal and the predicted location of the part adjacent to it in the body kinematic tree. The adjacent part location prediction is trained jointly with the part detector as in [12].

$\Delta_{ij}^{DM}$  is then defined as a ratio of number of point correspondences between the regions  $R_i$  and  $R_j$  and the total number of point correspondences in either of them. Specifically, let  $C = \{c^k | k = 1, \dots, K\}$  be a set of point correspondences between the two images computed with DeepMatching, where  $c^k = (c_1^k, c_2^k)$  and  $c_1^k$  and  $c_2^k$  denote the corresponding points in the first and second image respectively. Using this notation we define:

$$\Delta_{ij}^{DM} = \frac{|\{c^k | c_1^k \in R_i \wedge c_2^k \in R_j\}|}{|\{c^k | c_1^k \in R_i\}| + |\{c^k | c_2^k \in R_j\}|}. \quad (7)$$

The rationale behind computing  $\Delta_{ij}^{DM}$  by aggregating across multiple correspondences is to make the feature robust to outliers and to inaccuracies in body part detection.  $\tilde{\Delta}_{ij}^{DM}$  is defined analogously, but using the DeepMatching correspondences obtained by inverting the order of images.

**Discussion.** As we demonstrate in Sec. 4, we found the set of features described above to be complementary to each other. Euclidean distance between proposals is informative for finding correspondences for slow motions, but fails for faster motions and in the presence of multiple people. DeepMatching is usually effective in finding corresponding regions between the two images, but occasionally fails in the case of sudden background changes due to fast motion or large changes in body limb orientation. In these cases SIFT is often still able to provide a meaningful measure of similarity due to its rotation invariance.

## 4. Experiments

We perform evaluation of the proposed single-frame and video-based approaches after introducing datasets and the evaluation measure.

### 4.1. Datasets and evaluation measure

**Single frame.** We evaluate our single-frame models on the MPII Human Pose (Multi-Person) dataset [1]. It consists of 3844 training and 1758 testing groups of multiple overlapping people in highly articulated poses with a variable number of parts. We report all intermediate results on a validation set of 200 images sampled uniformly at random and refer to it as MPII Multi-Person Val, while major results and comparison to the state of the art are reported on the test set.

**Video.** In order to evaluate video-based models we introduce a novel dataset. To this end we manually selected challenging keyframes from MPII Human Pose (Multi-Person Test) dataset. Selected keyframes represent crowded scenes with highly articulated people engaging in various dynamic activities. In addition to each keyframe, we include +/-10 neighboring frames from the corresponding publicly available video sequences, and annotate every second frame<sup>5</sup>.

<sup>5</sup>The annotations in the original key-frame are kept unchanged.

Each body pose was annotated following the standard annotation procedure [1], while maintaining the identity of each individual throughout the sequence. In contrast to MPII Multi-Person where some frames may contain non-annotated people, in our dataset we annotate all people participating in the activity captured in the video, and add ignore regions for areas that contain dense crowds (e.g. static spectators in the dancing sequences). In total, our dataset consists of 28 sequences with over 2,000 annotated poses in total. We will release the dataset to the public.

**Evaluation details.** Evaluation on all datasets is performed on a per-frame basis. The average precision (AP) measure [19] is used for performance comparison. Additionally, for each algorithm we report the time in seconds per frame (s/f) it takes for the graph partitioning step to converge. All time measurements were conducted on a single core Intel Xeon 2.70GHz. Note that the actual run-time of each method might be somewhat longer due to the constant time steps such as computation of part proposals and pairwise terms. Evaluation on our Multi-Person Video dataset is performed on the full frames using the publicly available evaluation kit of [1]. On MPII Multi-Person we follow the official evaluation protocol<sup>6</sup> and evaluate on groups using the provided rough group location and scale.

## 4.2. Single-frame models

**Bottom-Up.** We consider different variants of our *Bottom-Up* model (c.f. Sec. 3.1) that (1) uses regression pairwise in a fully-connected graph of up to 1,000 detection proposals and infers both partitioning and labeling of detection proposals, similar to [12] (*BU-full, label*); (2) same as (1), but only partitioning is inferred, whereas the labeling of detection proposals is performed using highest detection score (*BU-full*); (3) same as (2) but uses a sparsely-connected graph (*BU-sparse*). Results are shown in Tab. 1. *BU-full, label* achieves 70.5% AP with a median run-time of 1.48 seconds/frame (s/f). *BU-full* achieves 11× run-time reduction (0.13 vs. 1.48 s/f): pre-labeling detection candidates based on part detection score allows to dramatically reduce the number of variables in the problem graph. Interestingly, pre-labeling also improves the performance (71.9 vs. 70.5% AP). The intuition is that some of the low-scoring detections may confuse the solver that tries to find an optimal part labeling based on detection scores. *BU-sparse* achieves further reduction in run-time (0.07 vs. 0.13 s/f), as it reduces the complexity of the initial problem by sparsifying the graph, at a price of a drop in performance (70.6 vs. 71.9% AP).

**Top-Down/Bottom-Up.** The results are shown in Tab. 2. Proposed *TD* achieves 71.7% AP. Interestingly, its performance is on par with more complex *BU-full*. This under-

Setting	Head	Sho	Elb	Wri	Hip	Knee	Ank	AP	time, [s/f]
<i>BU-full, label</i>	90.0	84.9	71.1	58.4	69.7	64.7	54.7	70.5	1.48
<i>BU-full</i>	91.2	86.0	<b>72.9</b>	61.5	70.4	65.4	55.5	71.9	0.13
<i>BU-sparse</i>	91.1	<b>86.5</b>	70.7	58.1	69.7	64.7	53.8	70.6	0.07
<i>TD/BU + SP</i>	<b>92.2</b>	86.1	72.8	<b>63.0</b>	<b>74.0</b>	<b>66.2</b>	<b>58.4</b>	<b>73.3</b>	<b>0.01</b>

Table 1. Effects of various variants of *BU* model on pose estimation performance (AP) on MPII Multi-Person Val.

Setting	Head	Sho	Elb	Wri	Hip	Knee	Ank	AP
<i>TD</i>	91.6	84.7	<b>72.9</b>	<b>63.2</b>	72.3	64.7	52.8	71.7
<i>TD + SP</i>	90.7	85.0	72.0	63.1	73.1	65.0	58.3	72.5
<i>TD/BU + SP</i>	<b>92.2</b>	<b>86.1</b>	72.8	63.0	<b>74.0</b>	<b>66.2</b>	<b>58.4</b>	<b>73.3</b>

Table 2. Effects of various versions of *TD/BU* model on pose estimation performance (AP) on MPII Multi-Person Val.

Setting	Head	Sho	Elb	Wri	Hip	Knee	Ank	AP	time [s/f]
<i>BU-full</i>	<b>91.5</b>	<b>87.8</b>	74.6	62.5	72.2	65.3	56.7	72.9	0.12
<i>TD/BU + SP</i>	88.8	87.0	<b>75.9</b>	<b>64.9</b>	<b>74.2</b>	<b>68.8</b>	<b>60.5</b>	<b>74.3</b>	<b>0.005</b>
<i>DeeperCut</i> [12]	79.1	72.2	59.7	50.0	56.0	51.0	44.6	59.4	485
<i>DeeperCut</i> [13]	89.4	84.5	70.4	59.3	68.9	62.7	54.6	70.0	485
Iqbal&Gall [14]	58.4	53.9	44.5	35.0	42.2	36.7	31.1	43.1	10

Table 3. Pose estimation results (AP) on MPII Multi-Person Test.

lines the advantages of the proposed strategy of offloading the larger share of the reasoning about body-part association onto the feed-forward convolutional architecture. Explicit spatial propagation (*TD+SP*) further improves the results (72.5 vs. 71.7% AP). The largest improvement is observed for ankles: progressive prediction that conditions on the close-by parts in the tree hierarchy reduces the distance from the conditioning location and location of the conditioned body part thereby simplifying the prediction task. Performing inference (*TD/BU+SP*) further improves the performance to 73.3% AP, as it allows for more optimal assignment of part detection candidates to corresponding persons. Due to the star connectivity in the *TD/BU* graph, inference time is reduced even further (0.01 vs. 0.07 for *BU-sparse*). Overall we observe very good pose prediction results with our simple and efficient person conditioned *Top-Down/Bottom-Up* model.

**Comparison to the State of the Art.** The proposed single-frame approaches are evaluated on the MPII Multi-Person dataset and compared to the state of the art [13] in Tab. 3. We observe that both *BU-full* and *TD/BU* models improve over the best published result of *DeeperCut* [13], achieving 72.9 and 74.3% AP respectively vs. 70.0% AP by *DeeperCut*. For the *TD/BU* approach the improvements on articulated parts (elbows, wrists, ankles, knees) are especially pronounced. We argue that this is due to using the network that is directly trained to disambiguate body parts of different people, instead of using explicit geometric pairwise terms that only serve as a proxy to person’s identity. Overall, the performance of our best approach *TD/BU* is noticeably higher (74.3 vs. 70.0% AP). Remarkably, inference

<sup>6</sup><http://human-pose.mpi-inf.mpg.de/#evaluation>



Figure 6. Qualitative comparison of results using single frame based model ( $BU\text{-sparse}$ ) vs. articulated tracking ( $BU\text{-sparse}+\text{temporal}$ ). See <http://youtube.com/watch?v=eYtn13fzGG0> for the supplemental material showcasing our results.

run-time in our least complex  $TD/BU$  approach is 5 orders of magnitude faster compared to *DeeperCut*. This speed-up is a combination of two factors. First, we are relying on a faster solver from [16] that tackles the graph-partitioning problem via local search, in contrast to the integer-linear program solver used in [12]. Second, in the case of  $TD/BU$  model the graph is sparse and a large portion of the computation is performed by the feed-forward convolutional network introduced in Sec. 3.2.

### 4.3. Multi-frame models

**Comparison of video-based models.** Performance of the proposed video-based models is compared in Tab. 4. Overall we observe that video-based models outperform single-frame models in each case.  $BU\text{-full}+\text{temporal}$  slightly outperforms  $BU\text{-full}$ , where improvements are noticeable for ankle, knee and head. Video-based  $BU\text{-sparse}+\text{temporal}$  noticeably improves over  $BU\text{-sparse}$  (73.1 vs. 71.6% AP). We observe significant improvements on the most difficult body parts such as ankles (+3.9% AP) and wrists (+2.6% AP). Interestingly,  $BU\text{-sparse}+\text{temporal}$  outperforms  $BU\text{-full} + \text{temporal}$ : longer-range connections such



Setting	Head	Sho	Elb	Wri	Hip	Knee	Ank	AP
<i>BU-full</i>	84.0	83.8	73.0	61.3	74.3	67.5	58.8	71.8
+ <i>temporal</i>	84.9	83.7	72.6	61.6	74.3	68.3	59.8	72.2
<i>BU-sparse</i>	84.5	84.0	71.8	59.5	<b>74.4</b>	68.1	59.2	71.6
+ <i>temporal</i>	<b>85.6</b>	84.5	73.4	62.1	73.9	68.9	63.1	73.1
<i>TD/BU+ SP</i>	82.2	85.0	75.7	64.6	74.0	69.8	62.9	73.5
+ <i>temporal</i>	82.6	<b>85.1</b>	<b>76.3</b>	<b>65.5</b>	74.1	<b>70.7</b>	<b>64.7</b>	<b>74.2</b>

Table 4. Pose estimation results (AP) on our Multi-Person Video.

as *e.g.* head to neck may introduce additional confusion when information is propagated over time. Finally, *TD/BU+temporal* improves over *TD/BU* alone (+0.7% AP). Similarly to *BU-sparse+temporal*, improvement is most prominent on ankles (+1.8% AP) and wrists (+0.9% AP). It is worth noting, that even the single-frame version of *TD/BU* outperforms the best temporal *BU* model. This is in line with our findings for single-frame models that demonstrate benefits of employing the convnet to directly perform multi-person inference.

We show examples of articulated tracking results on our video dataset in Fig. 6. Temporal reasoning helps in cases when image information is ambiguous due to close proximity of multiple people. For example the video-based approach succeeds in correctly localizing legs of the person in Fig. 6 (d), (h) and (l). Video typically helps more in difficult scenes with occlusions such as the first and second sequences in Fig. 6, but helps less in cases such as the third sequence when single-frame approach already performs rather well.

**Evaluation of temporal features.** We evaluate the importance of combining temporal features introduced in Sec. 3.4 on our Multi-Person Video dataset. To that end, we consider *BU-sparse+temporal* model and compare results to *BU-sparse* in Tab. 5. Single-frame *BU-sparse* achieves 71.6% AP. It can be seen that using geometry based *det-distance* features slightly improves the results to 72.1% AP, as it enables the propagation of information from neighboring frames. Using *deepmatch* features slightly improves the performance further as it helps to link the same body part of the same person over time based on the body part appearance. It is especially helpful in the case of fast motion where *det-distance* may fail. The combination of both geometry and appearance based features further improves the performance to 72.5%, which shows their complementarity. Finally, adding the *sift-distance* feature improves the results to 73.1%, since it copes better with the sudden changes in background and body part orientations. Overall, using a combination of temporal features in *BU-sparse+temporal* results in a 1.5% AP improvement over the single-frame *BU-sparse*. This demonstrates the advantages of the proposed approach to improve pose estimation performance using temporal information.

Setting	Head	Sho	Elb	Wri	Hip	Knee	Ank	AP
<i>BU-sparse</i>	84.5	84.0	71.8	59.5	74.4	68.1	59.2	71.6
+ <i>det-distance</i>	84.8	84.3	72.9	61.8	74.1	67.4	59.1	72.1
+ <i>deepmatch</i>	85.5	83.9	73.0	62.0	74.0	68.0	59.5	72.3
+ <i>det-distance</i>	85.1	83.6	72.2	61.5	<b>74.4</b>	68.8	62.2	72.5
+ <i>sift-distance</i>	<b>85.6</b>	<b>84.5</b>	<b>73.4</b>	<b>62.1</b>	73.9	<b>68.9</b>	<b>63.1</b>	<b>73.1</b>

Table 5. Effects of different temporal features on pose estimation performance (AP) (*BU-sparse+temporal* model) on our Multi-Person Video dataset.

## 5. Conclusion

In this paper we introduced an efficient and effective approach to articulated human pose estimation and tracking in monocular video. Our approach defines a model that jointly groups body part proposals within each video frame and across time. Grouping is formulated as a graph partitioning problem that lends itself to efficient inference with recent local search techniques. Our approach improves over state-of-the-art while being substantially faster compared to other related work.

**Acknowledgements.** This work has been supported by the Max Planck Center for Visual Computing and Communication. The authors would like to thank Varvara Obolonchikova and Bahar Tarakameh for their help in creating the video dataset.

## Appendix: Additional Results on the MPII Multi-Person Dataset

We perform qualitative comparison of the proposed single-frame based *TD/BU* and *BU-full* methods on challenging scenes containing highly articulated and strongly overlapping individuals. Results are shown in Fig. 7 and Figure 8. The *BU-full* works well when persons are sufficiently separated (images 11 and 12). However, it fails on images where people significantly overlap (images 1-3, 5-10) or exhibit high degree of articulation (image 4). This is due to the fact that geometric image-conditioned pairwise may get confused in the presence of multiple overlapping individuals and thus mislead post-CNN bottom-up assembling of body poses. In contrast, *TD/BU* performs explicit modeling of person identity via top-down bottom-up reasoning while offloading the larger share of the reasoning about body-part association onto feed-forward convolutional architecture, and thus is able to resolve such challenging cases. Interestingly, *TD/BU* is able to correctly predict lower limbs of people in the back through partial occlusion (image 3, 5, 7, 10). *TD/BU* model occasionally incorrectly assembles body parts in kinematically implausible manner (image 12), as it does not explicitly model geometric body part relations. Finally, both models fail in presence of high variations in scale (image 13). We envision that reasoning over multiple scales is likely to improve the results.

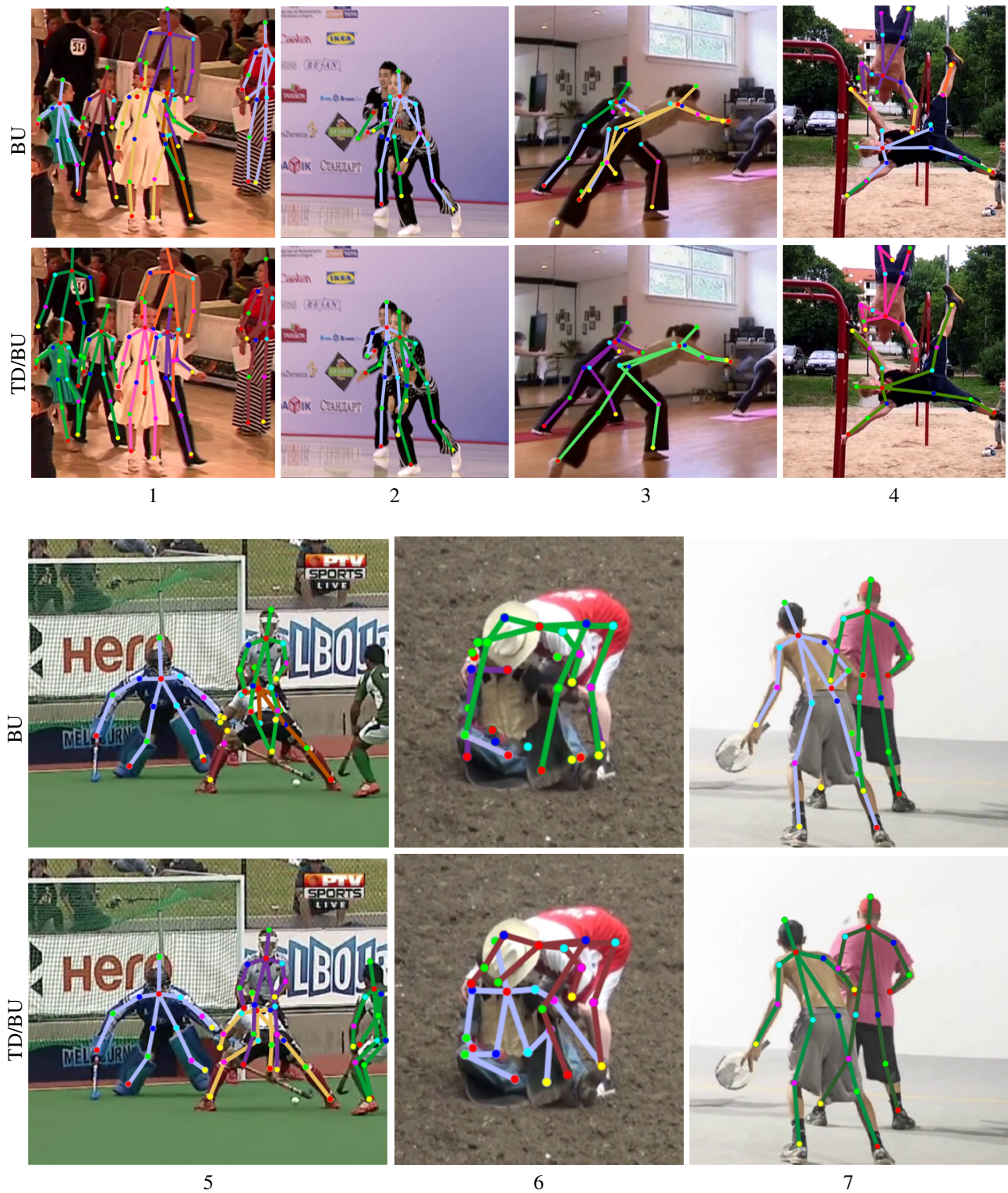


Figure 7. Qualitative comparison of single-frame based *TD/BU* and *BU-full* on MPII Multi-Person dataset.

## References

- [1] M. Andriluka, L. Pishchulin, P. Gehler, and B. Schiele. 2d human pose estimation: New benchmark and state of the art analysis. In *CVPR'14*. 6, 7
- [2] M. Andriluka, S. Roth, and B. Schiele. People-tracking-by-



Figure 8. Successful (8-11) and failure (12-13) pose estimation results by single-frame based *TD/BU* and comparison to *BU-full* on MPII Multi-Person dataset.

- detection and people-detection-by-tracking. In *CVPR'08*. 2
- [3] M. Andriluka, S. Roth, and B. Schiele. Monocular 3d pose estimation and tracking by detection. In *CVPR*, 2010. 2
- [4] A. Bulat and G. Tzimiropoulos. Human pose estimation via convolutional part heatmap regression. In *ECCV'16*. 2
- [5] J. Charles, T. Pfister, D. Magee, and A. Hogg, D. Zisserman. Personalizing human video pose estimation. In *CVPR'16*. 2
- [6] L.-C. Chen, G. Papandreou, I. Kokkinos, K. Murphy, and A. L. Yuille. Semantic image segmentation with deep convolutional nets and fully connected crfs. In *ICLR*, 2015. 5
- [7] A. Cherian, J. Mairal, K. Alahari, and C. Schmid. Mixing body-part sequences for human pose estimation. In *CVPR'14*. 2
- [8] A. Elhayek, E. Aguiar, A. Jain, J. Tompson, L. Pishchulin, M. Andriluka, C. Bregler, B. Schiele, and C. Theobalt. Efficient convnet-based marker-less motion capture in general scenes with a low number of cameras. In *CVPR'15*. 2
- [9] A. Elhayek, E. Aguiar, A. Jain, J. Tompson, L. Pishchulin, M. Andriluka, C. Bregler, B. Schiele, and C. Theobalt. Marconi - convnet-based marker-less motion capture in outdoor and indoor scenes. 2

- [10] G. Gkioxari, A. Toshev, and N. Jaitly. Chained predictions using convolutional neural networks. [2](#)
- [11] K. He, X. Zhang, S. Ren, and J. Sun. Deep residual learning for image recognition. *arXiv preprint arXiv:1512.03385*, 2015. [5](#)
- [12] E. Insafutdinov, L. Pishchulin, B. Andres, M. Andriluka, and B. Schiele. Deeppercut: A deeper, stronger, and faster multi-person pose estimation model. In *ECCV'16*. [2](#), [3](#), [4](#), [5](#), [6](#), [7](#), [8](#)
- [13] E. Insafutdinov, L. Pishchulin, B. Andres, M. Andriluka, and B. Schiele. Deeppercut: A deeper, stronger, and faster multi-person pose estimation model. *arXiv preprint arXiv:1605.03170*. [7](#)
- [14] U. Iqbal and J. Gall. Multi-person pose estimation with local joint-to-person associations. In *ECCVw'16*. [2](#), [7](#)
- [15] Y. Jia, E. Shelhamer, J. Donahue, S. Karayev, J. Long, R. Girshick, S. Guadarrama, and T. Darrell. Caffe: Convolutional architecture for fast feature embedding. *arXiv preprint arXiv:1408.5093*, 2014. [6](#)
- [16] E. Levinkov, S. Tang, E. Insafutdinov, and B. Andres. Joint graph decomposition and node labeling by local search. *arXiv preprint arXiv:1611.04399*. [2](#), [3](#), [4](#), [5](#), [8](#)
- [17] A. Newell, K. Yang, and J. Deng. Stacked hourglass networks for human pose estimation. In *ECCV'16*. [2](#)
- [18] T. Pfister, J. Charles, and A. Zisserman. Flowing convnets for human pose estimation in videos. In *ICCV'15*. [2](#)
- [19] L. Pishchulin, E. Insafutdinov, S. Tang, B. Andres, M. Andriluka, P. Gehler, and B. Schiele. Deepcut: Joint subset partition and labeling for multi person pose estimation. In *CVPR'16*. [1](#), [2](#), [3](#), [4](#), [7](#)
- [20] B. Sapp, D. Weiss, and B. Taskar. Parsing human motion with stretchable models. In *CVPR'11*. [2](#)
- [21] S. Tang, B. Andres, M. Andriluka, and B. Schiele. Subgraph decomposition for multi-target tracking. In *CVPR*, 2015. [1](#), [2](#), [3](#), [4](#), [5](#)
- [22] S. Tang, B. Andres, M. Andriluka, and B. Schiele. Multi-person tracking by multicuts and deep matching. In *BMTT*, 2016. [6](#)
- [23] R. Tokola, W. Choi, and S. Savarese. Breaking the chain: liberation from the temporal markov assumption for tracking human poses. In *ICCV'13*. [2](#)
- [24] J. J. Tompson, A. Jain, Y. LeCun, and C. Bregler. Joint training of a convolutional network and a graphical model for human pose estimation. In *NIPS'14*. [2](#)
- [25] S.-E. Wei, V. Ramakrishna, T. Kanade, and Y. Sheikh. Convolutional pose machines. In *CVPR'16*. [2](#)
- [26] P. Weinzaepfel, J. Revaud, Z. Harchaoui, and C. Schmid. Deepflow: Large displacement optical flow with deep matching. In *ICCV'13*. [6](#)
- [27] D. J. Weiss and B. Taskar. Learning adaptive value of information for structured prediction. In *NIPS'13*. [2](#)